Difference in the Mechanisms of the Cold and Heat Induced Unfolding of Thioredoxin *h* from *Chlamydomonas reinhardtii*: Spectroscopic and Calorimetric Studies[†]

John M. Richardson, III,[‡] Stéphane D. Lemaire,[§,||] Jean-Pierre Jacquot,[§,⊥] and George I. Makhatadze*[,‡]

Department of Biochemistry and Molecular Biology, Penn State College of Medicine, Hershey, Pennsylvania 17033, and Institut de Biotechnologie des Plantes, URA 1128 CNRS, Université de Paris-Sud, Bâtiment 630, 91405 Orsay Cedex, France

Received March 17, 2000; Revised Manuscript Received June 13, 2000

ABSTRACT: The thermodynamic stability and temperature induced structural changes of oxidized thioredoxin *h* from *Chlamydomonas reinhardtii* have been studied using differential scanning calorimetry (DSC), near- and far-UV circular dichroism (CD), and fluorescence spectroscopies. At neutral pH, the heat induced unfolding of thioredoxin *h* is irreversible. The irreversibly unfolded protein is unable to refold due to the formation of soluble high-order oligomers. In contrast, at acidic pH the heat induced unfolding of thioredoxin *h* is fully reversible and thus allows the thermodynamic stability of this protein to be characterized. Analysis of the heat induced unfolding at acidic pH using calorimetric and spectroscopic methods shows that the heat induced denaturation of thioredoxin *h* can be well approximated by a two-state transition. The unfolding of thioredoxin *h* is accompanied by a large heat capacity change [6.0 ± 1.0 kJ/(mol·K)], suggesting that at low pH a cold denaturation should be observed at the above-freezing temperatures for this protein. All used methods (DSC, near-UV CD, far-UV CD, Trp fluorescence) do indeed show that thioredoxin *h* undergoes cold denaturation at pH <2.5. The cold denaturation of thioredoxin *h* cannot, however, be fitted to a two-state model of unfolding. Furthermore, according to the far-UV CD, thioredoxin *h* is fully unfolded at pH 2.0 and 0 °C, whereas the other three methods (near-UV CD, fluorescence, and DSC) indicate that under these conditions 20−30% of the protein molecules are still in the native state. Several alternative mechanisms explaining these results such as structural differences in the heat and cold denatured state ensembles and the two-domain structure of thioredoxin *h* are discussed.

Thioredoxins are ubiquitous 100−120 amino acid residue proteins found in all living organisms including photosynthetic and nonphotosynthetic bacteria, algae, higher plants, and vertebrates (*1*). Such a broad distribution of thioredoxin is presumably linked to its function as a disulfide bond reductase of selected target proteins and enzymes (*1*−*4*).

Three-dimensional structures of thioredoxins from different organisms have been determined by X-ray and NMR spectroscopies: *Escherichia coli* (*5*−*8*), human (*9*−*11*), *Chlamydomonas reinhardtii* (*12*−*14*), *Bacillus acidocaldarius* (*15*), and *Anabaena* sp. (*16*). The secondary and tertiary structures display a thioredoxin fold which is shared by several other proteins (*3, 4*). The small size, the availability of three-dimensional structures, and the high solubility make this protein an attractive model for the study of conformational properties (*17*−*25*) and for the protein engineering and design purposes (*26*−*28*).

Two different thioredoxin genes have been isolated in the unicellular green alga *Chlamydomonas reinhardtii* (*1*). The products of these genes, thioredoxin *h* and thioredoxin *m*, share ∼50% sequence similarities (*1*). Thioredoxins *h* and *m* are located in two different subcellular compartments, namely, the cytosol and the chloroplast. Accordingly, they are reduced by different mechanisms: the cytosolic protein via NADPH and the flavoenzyme NADPH thioredoxin reductase, and the chloroplast protein through a cascade comprising the photosynthetic electron transport and the soluble stromal proteins ferredoxin and ferredoxin−thioredoxin reductase. Besides the different modes of reduction, the two isoproteins display differential selectivity versus their target enzymes. Thioredoxin *m* is an efficient reducer and activator of NADP−malate dehydrogenase and several enzymes of the oxidative pentose phosphate cycle, but can also deactivate plastidic glucose-6-phosphate dehydrogenase. On the other hand, the physiological acceptors of thioredoxin *h* are less well described. One of those could be a recently described cytosolic thiol-dependent peroxidase. Thioredoxin *m* is believed to control the oxidative pentose phosphate pathway in chloroplasts and to function as an antioxidant in this organelle. Thioredoxin *h*, on the other hand, could play a role as a signal molecule since it is one of the major proteins translocated in the phloem sap in higher plants. References dealing with the physiological aspects of thioredoxin in photosynthetic organisms can be found in (*1*).

[†] Supported in part by a grant from the NIH (GM54537 to G.I.M.).
* To whom correspondence should be addressed. E-mail: makhatadze@psu.edu, Phone: (717) 531-0712, Fax: (717) 531-7072.
[‡] Penn State College of Medicine.
[§] Université de Paris-Sud.
[||] Current address: Department of Molecular Biology and Plant Biology, Sciences II, University of Geneva, CH-1211, Geneva, Switzerland.
[⊥] Current address: Laboratoire de Biologie Forestière, Université de Nancy I, 54506 Vandoeuvre, France.

10.1021/bi000610b CCC: $19.00
Published on Web 08/17/2000

The 3D structures for thioredoxin *h* (*13, 14*) and thioredoxin *m* (*1, 12*) are also quite similar, and consist of five β-strands and four α-helices. Nevertheless, the physicochemical properties of these two proteins differ remarkably in terms of both the absorption spectra and the pH/temperature aggregation properties (*29*). To better understand the similarities and differences of these two proteins, we studied the conformational stability of thioredoxin *h* using differential scanning calorimetry, far- and near-UV circular dichroism spectroscopies, and fluorescence spectroscopy. Combination of these calorimetric and spectroscopic methods has permitted us to show that at acidic pH Trx *h*[1] can be unfolded by both increasing and decreasing the temperature from ambient; i.e., it can undergo both heat and cold denaturation. The heat induced unfolding of Trx *h* can be well approximated by a two-state unfolding. The cold induced unfolding, however, cannot be fitted to a two-state model. Based on this result, we propose that thioredoxin *h* consists of two thermodynamic domains. These domains strongly interact (high cooperativity) at high temperature, leading to a two-state behavior of the system. At low temperatures, however, the interactions between domains in Trx *h* are weakened (low cooperativity), thus leading to a non-two-state behavior. This model is supported by experimentally observed three-state heat induced unfolding of thioredoxin *m*.

MATERIALS AND METHODS

Protein Expression and Purification. Thioredoxin *h* and thioredoxin *m* were overexpressed in *Escherichia coli* and purified to apparent homogeneity as described earlier (*29*). Both proteins were stored at −20 °C as ammonium sulfate precipitates in 50 mM Tris-HCl, pH 7.0, buffer.

Sample Preparation. Ammonium sulfate precipitated Trx *h* was diluted severalfold and dialyzed against four changes of water followed by dialysis against two changes of the buffer. Buffers used were 10 mM sodium phosphate at pH 7.0 or 10 mM glycine/HCl for the pH range from 2.0 to 3.5. All buffer solutions were filtered using 0.45 μm polyethersulfone filter membranes. Insoluble material was removed from the protein solution by centrifugation for at least 15 min at 13000*g*. Protein concentration was determined spectrophotometrically using an extinction coefficient of $E^{1cm}_{0.1\%,280nm} = 1.211$ for Trx *h* and $E^{1cm}_{0.1\%,280nm} = 1.326$ for Trx *m*, calculated according to Gill and von Hippel (*30*) as described (*31*). Light scattering was corrected according to Winder and Gent (*32*).

Circular Dichroism Spectroscopy. Circular dichroism (CD) measurements were performed either with a JASCO J-20 spectropolarimeter equipped with photoelastic modulator and lock-in amplifier or with a JASCO J-715. The details of the measurement procedures are described elsewhere (*33, 34*). Quartz cells with 1 mm (far-UV) and 5 or 10 mm (near-UV) light path length were used. The temperature of the thermostated cell holder was controlled with a circulated water bath programmed to raise the temperature at a rate of 60 °C/h. The protein concentration was between 0.1 and 0.3 mg/mL for far-UV CD, and 2−4 mg/mL for near-UV CD experiments.

Fluorescence Spectroscopy. Fluorescence measurements were performed using a FluoroMax spectrofluorometer with DM3000F software in 1 cm cells as described (*35*). Temperature induced unfolding was followed by monitoring the changes in the tryptophan fluorescence intensity at 330 nm after excitation at 295 nm. The temperature of the thermostated cell holder was controlled with a circulated water bath programmed to raise the temperature by 0.7 °C/min. The protein concentration in all cases was 0.014 mg/mL. Because the intrinsic Trp fluorescence intensity strongly depends on temperature and this dependence is nonlinear, it is difficult to get estimates of the temperature dependences of the native and unfolded baselines. Thus, to get an estimate of the temperature dependencies of the native and unfolded states, we used the model compound *N*-acetyltryptophanamide (NATA). The temperature dependence of the fluorescence intensity change for 23 μM NATA (the same molar concentration as that of Trp residues in Trx *h*) was recorded under conditions identical to the protein experiments. The changes of the fluorescence intensity of NATA with temperature appeared to be well described by a second-order polynomial, $I_{NATA}(T)$. This polynomial was used to define the temperature dependencies of the fluorescence intensity of the native, $I_N(T)$, and unfolded, $I_U(T)$, states as

$$I_N(T) = A_N + B_N \cdot I_{NATA}(T) \quad (1)$$

$$I_U(T) = B_U \cdot I_{NATA}(T) \quad (2)$$

where A_N, B_N, and B_U are the fitted parameters, obtained using simultaneous fitting of several melting profiles (see below).

Differential Scanning Calorimetry. The calorimetric experiments were performed on VP-DSC by Microcal Inc. (*36*). All experiments were performed at a heating rate of 1 °C/min, although some experiments were performed at a heating rate of 0.5 °C/min without any notable effect on the calorimetric profiles. Protein concentrations for the calorimetric experiments varied from 0.4 to 3 mg/mL. The partial molar volume of Trx *h* required for the calculation of the partial molar heat capacity was taken to be 0.738 mL/g according to Makhatadze at al. (*37*).

Data Analysis. Changes in the spectroscopic signal (fluorescence intensity, CD at 222 nm, or CD at 300 nm) as a function of temperature, $Y_x(T)$, have been analyzed in terms of a two-state model. The fraction of the native and unfolded proteins is defined by the experimental observable $Y_x(T)$ as

$$F_N = 1 - F_U = \frac{Y_x(T) - Y_U(T)}{Y_N(T) - Y_U(T)} \quad (3)$$

where $Y_N(T)$ and $Y_U(T)$ are the temperature dependencies of the experimental observable for native and unfolded states, respectively, and $F_N(T)$ and $F_U(T)$ are the fractions of protein in the native and unfolded states, respectively. The spectroscopic signals for the native and unfolded states are considered to be linear functions of temperature in the case of CD at both far-UV or near-UV CD or by nonlinear functions of temperature as in eqs 4 and 5 for the fluorescence intensity. The fraction of protein in the unfolded state

[1] Abbreviations: Trx *h*, thioredoxin *h* from *Chlamydomonas reinhardtii*; Trx *m*, thioredoxin *m* from *Chlamydomonas reinhardtii*; DSC, differential scanning calorimetry; CD, circular dichroism spectroscopy.

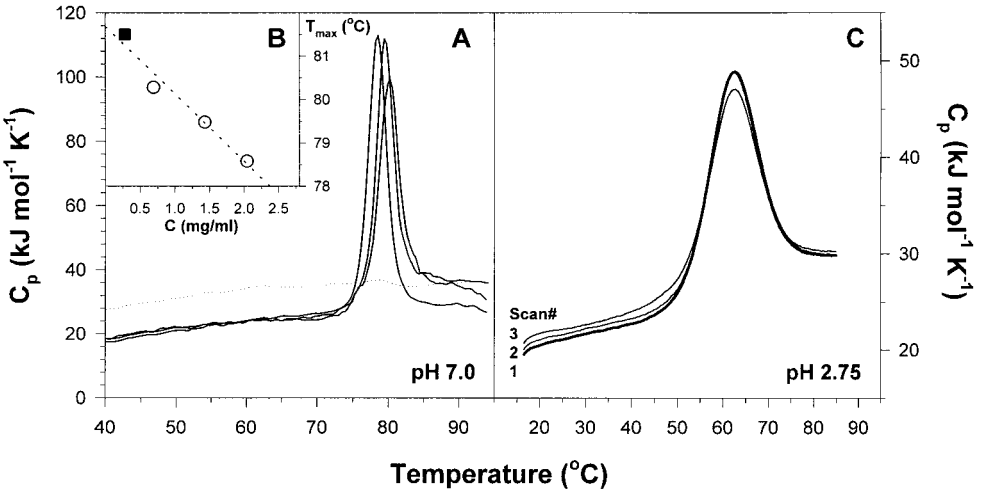

FIGURE 1: (A) Effect of protein concentration on the irreversible temperature induced transition profiles as monitored by DSC for Trx *h* in 10 mM sodium phosphate buffer, pH 7.0. Concentrations are 0.6, 1.43, and 2.04 mg/mL. Dashed lines show the temperature dependence of the partial molar heat capacity of Trx *h* (0.6 mg/mL) upon reheating. (B) Dependence of the apparent transition temperature on the concentration of Trx *h* at pH 7.0: open circles, data obtained using DSC; filled square, data from the temperature induced unfolding monitored by Trp fluorescence. (C) Reversibility of the temperature induced transition of Trx *h* in 10 mM glycine buffer, pH 2.75. Thin lines show three consequent reheats of the same sample.

is related to the equilibrium constant for a two-state transition, *K*, as

$$F_U(T) = 1 - F_N(T) = \frac{K}{1+K} \quad (4)$$

The equilibrium constant is expressed as

$$K = \exp\left(\frac{-[\Delta H(T) - T\cdot\Delta S(T)]}{R\cdot T}\right) \quad (5)$$

where $\Delta H(T)$ and $\Delta S(T)$ are the enthalpy and entropy functions, correspondingly. With the assumption of the temperature-independent heat capacity change upon protein unfolding, ΔC_p (*38*, *39*):

$$\Delta H(T) = \Delta H(T_m) + (T - T_m)\cdot\Delta C_p \quad (6)$$

and

$$\Delta S(T) = \Delta S(T_m) + \Delta C_p\cdot\ln(T/T_m) = \Delta H(T_m)/T_m + \Delta C_p\cdot\ln(T/T_m) \quad (7)$$

where T_m is the transition temperature defined as the temperature at which $F_N = F_U = 0.5$ and thus $\Delta G(T_m) = \Delta H(T_m) - T_m\cdot\Delta S(T_m) = 0$.

The analysis of the DSC melting profiles was performed according to a two-state model as described (*40*) with temperature-independent ΔC_p and linear temperature dependences for the heat capacities of the native and unfolded states. The data were also analyzed using a temperature-dependent ΔC_p and second-order polynomial for the temperature dependence of the unfolded state. Incorporation of these modifications into the fitting routine did not lead to a significant improvement in the quality of the fit and/or lead to the meaningless (negative) estimates of the enthalpy of unfolding and the ΔC_p function. The nonlinear regression to a three-state model was not stable because of the uncertainties associated with the heat capacity function of the intermediate state.

Several melting profiles obtained using a given spectroscopic method or DSC were fitted simultaneously using common temperature-dependent functions for the native and unfolded states, and a common value of the heat capacity change. The nonlinear fit was performed using program NLREG.

In cases where the contribution of cold denaturation is significant and results in less than 50% of the population of the native state at any temperature, the transition temperature, T_m, is undefined. Thus, the reference temperature was chosen as the temperature where the Gibbs energy function reaches a maximum; i.e., the entropy is zero (*41*).

RESULTS AND DISCUSSION

Reversibility of Trx h Unfolding. One of the most important prerequisites for the thermodynamic analysis of protein stability is the reversibility of the folding/unfolding reaction. Figure 1A presents the calorimetric profiles for the unfolding of Trx *h* at neutral pH. At this pH, the temperature induced unfolding is fully *irreversible*, and the reheating of the sample does not produce any observable heat absorption effects. No visible precipitation was observed on the irreversible sample. The cause of the irreversible step in the unfolding of Trx *h* appears to be aggregation of the unfolded state (*29*). Support for this conclusion can be also seen from the concentration dependence of the temperature at which the maximum of the heat absorption profile, T_{max}, is observed in heat capacity profiles. As the concentration of Trx *h* increases, the temperature of the maximum of the DSC profile decreases. This indicates a nonmonomolecular character of the unfolding reaction, i.e., $n\cdot M \rightarrow U_n$ (*40*, *42*). Linear extrapolation to zero concentration of protein provides an estimate of the thermostability of Trx *h* at pH 7.0 as 82 °C (Figure 1B). This agrees well with the thermostability estimates based on the activity measurements in these solvent conditions (*29*). For comparison, *E. coli* thioredoxin under similar solvent conditions undergoes a reversible unfolding with a transition temperature of 87 °C (*43*) whereas thio-

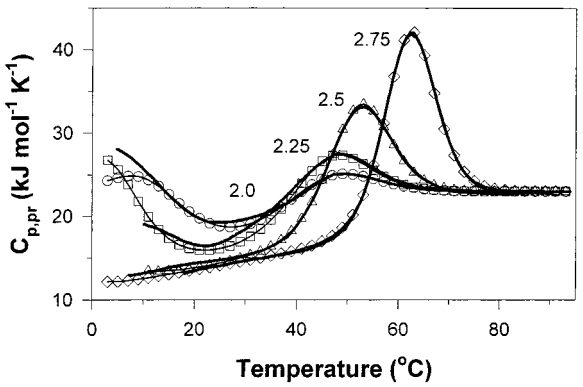

FIGURE 2: Profiles of heat-dependent unfolding of Trx *h* monitored by DSC (thick lines). Symbols (○, pH 2.0; □, pH 2.25; △, pH 2.5; ◇, pH 2.75) and thin lines show the results of the simultaneous fit of all profiles using the thermodynamic parameters shown in Table 1. pH values are also indicated above each curve.

Table 1: Thermodynamic Parameters of Unfolding of Trx *h* Obtained from Analysis of the DSC Data[a]

pH	T_m (°C)	ΔH_{cal} (kJ/mol)	ΔH_{fit} (kJ/mol)	$\Delta H_{cal}/\Delta H_{fit}$
2.00	28.1[b]	—[b]	0	–
2.25	40.0	–	127	–
2.50	51.1	220	219	1.01
2.75	59.8	280	281	0.99
3.00	66.4	324	330	0.98
3.25	73.6	338	348	0.97

[a] The estimated errors for the reported thermodynamic parameters are as follows: for the transition temperature, T_m, the error of measurements is less than 1 °C; for the calorimetric enthalpy of unfolding, ΔH_{cal} has an uncertainty of less than 5−7% and is largely due to the uncertainties of concentration measurements; the fitted enthalpy for a two-sate transition, ΔH_{fit}, has an error bar of less than 5 kJ/mol. [b] The underlined values do not represent the transition temperature but the temperature at which the entropy change is 0 (see Materials and Methods for details). In this case, the calorimetric enthalpy cannot be obtained experimentally.

redoxin from *Bacillus acidocaldarius* is even more thermostable and has a transition temperature of 103 °C (*44*).

The irreversible unfolding of Trx *h* was observed in the pH range from 7.0 to 4.0 (data not shown). However, at pH values lower than 3.5, the unfolding of Trx *h* becomes reversible; 90−100% recovery of the original heat capacity profile was observed not only for the second but also for the third reheat of the same sample (Figure 1C). This indicates that under acidic pH conditions (pH <3.5) the unfolding transition can be analyzed in terms of equilibrium thermodynamics.

Thermodynamic Parameters of Unfolding of Trx h at Acidic pH. The representative DSC profiles for reversible unfolding of Trx *h* at several pH values are shown in Figure 2. These profiles have been analyzed using a two-state model in which only native and unfolded states are populated (see Materials and Methods). The results of the analysis are presented in Table 1. In the pH range from 2.5 to 3.25, the experimental calorimetric enthalpy of unfolding is equal, within the experimental error, to the fitted enthalpy for the two-state transition (Table 1). This indicates a two-state mechanism for the heat-dependent unfolding transition in Trx *h*.

Figure 3 presents the dependence of the enthalpy of unfolding on the transition temperature, T_m. The slope of this function represents the heat capacity change upon unfolding, ΔC_p. The linear fit of the data in the pH range 2.5−3.25 provides a value of 6.0 ± 1.1 kJ·mol^{-1}·K^{-1} for the heat capacity change upon unfolding of Trx *h*. This estimate is similar to 5.9 ± 2.0 kJ·mol^{-1}·K^{-1} obtained from the simultaneous fit of all DSC profiles to a two-state model (see Materials and Methods). The obtained values for ΔC_p for Trx *h* are close, within experimental error, to the value of 7.0 ± 1.2 kJ·mol^{-1}·K^{-1} reported in (*43*) for the heat capacity of unfolding of *E. coli* thioredoxin. The enthalpy of unfolding of *E. coli* thioredoxin also compares well with the enthalpy of unfolding of Trx *h* (Figure 3). At 87 °C, the enthalpy of unfolding of *E. coli* thioredoxin is 435 kJ/mol, which is close to the value of 430 kJ/mol for the enthalpy of unfolding of Trx *h* at this temperature after extrapolation. A linear extrapolation of the enthalpy function of Trx *h* to the low-temperature range shows that the enthalpy will change sign at ∼20 °C. This temperature, which is also known as the inversion temperature, T_{inv}, is relatively high as compared to other proteins (*45*−*50*). High T_{inv} indicates that one can expect cold denaturation of Trx *h* at temperatures above the freezing point of aqueous solution (*41*). This explains the complex DSC profiles of Trx *h* at pH values of 2.25 and 2.00 (Figure 2); i.e., under these conditions Trx *h* undergoes cold denaturation.

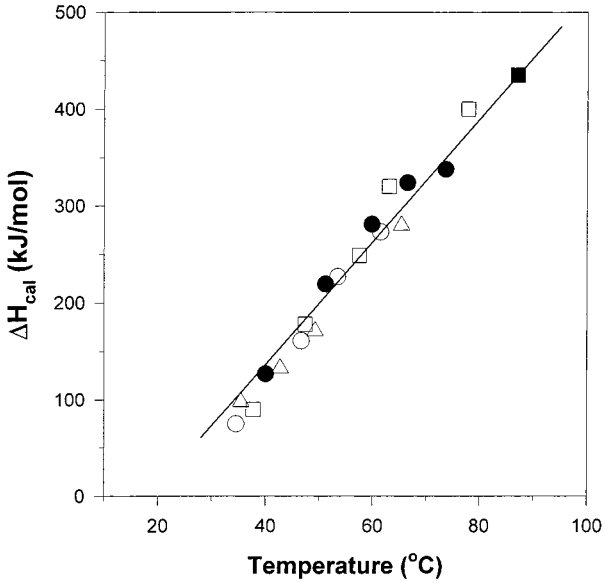

FIGURE 3: Dependence of the enthalpy of Trx *h* unfolding on temperature: (●) data obtained from DSC; (○) data obtained from the analysis of the near-UV CD melting profiles; (□) data obtained from the analysis of the far-UV CD melting profiles; (△) data obtained from the analysis of the fluorescence melting profiles. The slope of the line represents the heat capacity change upon unfolding, ΔC_p = 6.0 ± 1.1 kJ·mol^{-1}·K^{-1}. For comparison, (■) show the enthalpy of unfolding of *E. coli* thioredoxin at pH 7.0 taken from (*43*).

A two-state fit of the heat capacity profiles of Trx *h* at pH 2.0 and 2.25 is shown in Figure 2. The fit is qualitatively very good at the temperatures above 35 °C, i.e., the part of the profile representing the heat denaturation. However, the low-temperature (<35 °C) regions of the heat capacity profiles at pH 2.0 and 2.25 are very poorly fitted by a two-state model. Is this poor fit the result of an experimental artifact or is it an indication that the cold denaturation of Trx *h* is not a two-state process? To answer this question,

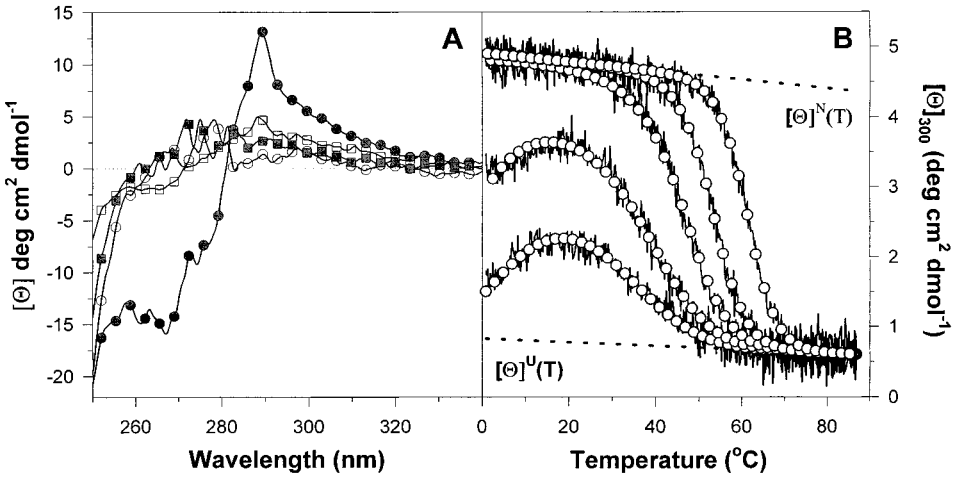

FIGURE 4: (Panel A) Comparison of the near-UV CD spectra of Trx *h* at different pHs and temperatures: (●) pH 3.0, 1 °C; (■) pH 3.0, 85 °C; (○) pH 2.0, 1 °C; (□) pH 2.0, 70 °C. (Panel B) Temperature induced unfolding profiles of Trx *h* at different pHs of solution monitored by the changes of ellipticity at 300 nm. Thin lines show actual experimental data, and dashed lines the temperature dependence of the ellipticities for the native, $[\Theta]^N(T)$, and unfolded, $[\Theta]^U(T)$, states. Open circles show the results of the global fit of all profiles to eq 8 using parameters shown in Table 2. The experiments were performed at pH values of (from left to right) 2.0, 2.25, 2.5, 2.75, and 3.0.

we performed the study of Trx *h* unfolding using circular dichroism and fluorescence spectroscopies.

Temperature Induced Conformational Changes in Trx h Monitored by Near-UV CD Spectroscopy. The near-UV CD spectroscopy is measuring the asymmetry in the environment of the aromatic residues (*51*). Since aromatic residues are usually buried in the interior of native protein, the changes in the near-UV CD spectrum are believed to represent the changes in the tertiary conformation. There are four phenylalanines, two tyrosines, and two tryptophans in the molecule of Trx *h* (*1*). Thus, one can expect that Trx *h* will have a well-pronounced spectrum in the near-UV CD. The spectrum of Trx *h* at pH 3.0 and 1 °C is shown in Figure 4A and has well-defined fine structure with a maximum at 290 nm and two small minima at 268 and 262 nm. The maximum of ellipticity at 290 nm can be attributed to Trp and Tyr residues and is often considered to be a diagnostic for a specific environment for these residues (*52*). Two minima, smaller in amplitude, at 268 and 262 nm are usually attributed to phenylalanine residues in a highly specific well-packed environment (*52*). Thus, overall the near-UV CD spectrum at pH 3.0 and 1 °C corresponds to a native protein. The fine structure of the spectrum disappears at high temperatures (80 °C) due to protein unfolding (Figure 4A).

Figure 4B shows the changes in the ellipticity of Trx *h* at 300 nm as a function of temperature at five pH values 2.0, 2.25, 2.5, 2.75, and 3.0. At the three highest pHs, 2.5, 2.75, and 3.0, the ellipticity profiles have a sigmoidal shape typical of a cooperative two-state unfolding. Under these conditions, the ellipticity at low temperature (<40 °C) is on the order of 5 deg·cm^2·dmol^{-1} and is weakly dependent on temperature. Upon unfolding of Trx *h*, the ellipticity decreases to ~1 deg·cm^2·dmol^{-1} and is weakly temperature dependent at high (>60 °C) temperatures. The ellipticity of Trx *h* at pH 2.0 and 2.25 follows similar patterns at high temperatures. At low temperatures, however, the ellipticity of Trx *h* at pH 2.0 and 2.25 is lower than the ellipticity of the native Trx *h* (5 deg·cm^2·dmol^{-1}). The shape of the ellipticity dependence on temperature at these pHs is also different. The ellipticity initially increases, approaching a maximum at ~20 °C followed by a decrease at high temperatures until it reaches the values similar to those recorded at higher pH. These results can be interpreted in terms of cold denaturation similarly to the DSC profiles shown in Figure 2.

Table 2: Thermodynamic Parameters of Unfolding of Trx *h* Computed from the Spectroscopic Data[a]

	method					
	far-UV CD (222 nm)		near-UV CD (300 nm)		fluorescence	
pH	T_m (°C)	$\Delta H(T_m)$ (kJ/mol)	T_m (°C)	$\Delta H(T_m)$ (kJ/mol)	T_m (°C)	$\Delta H(T_m)$ (kJ/mol)
2.00	26.0[b]	−1	19.0[b]	−1	19.5[b]	2
2.13	–	–	–	–	35.4	98
2.25	37.7	90	34.5	75	42.7	133
2.50	47.3	178	46.6	161	49.2	171
2.75	57.5	249	53.4	227	–	–
3.00	63.0	320	61.4	273	65.3	280

[a] The estimated errors for the reported thermodynamic parameters are as follows: for the transition temperature, T_m, the error of measurements is ±3−5 °C; and the fitted enthalpy for a two-sate transition, ΔH_{fit}, has an error bar of less than 5−7 kJ/mol. [b] The underlined values represent not the transition temperature but the temperature at which the entropy change is 0 (see Materials and Methods for details).

The temperature dependences of ellipticity of Trx *h* measured at different pH values were fitted simultaneously to a two-state model as

$$[\Theta]_{300}(T) = F_N(T)\cdot[\Theta]^N_{300}(T) + [1 - F_N(T)]\cdot[\Theta]^U_{300}(T) \quad (8)$$

where $[\Theta]^N_{300}(T)$ and $[\Theta]^U_{300}(T)$ are the ellipticities for the native and unfolded states, respectively, approximated by linear functions of temperature, and $F_N(T)$ is the temperature dependence of the population of the native protein defined by eqs 3 and 4. The results of the analysis are shown in Figure 4B and in Table 2. The calculated values of the enthalpy of unfolding as a function of temperature compare well the enthalpies of unfolding obtained from DSC (Figure 3). The overall quality of fit of the ellipticity to a two-state model is excellent at every pH (Figure 4B). This contrasts with the results of the analysis of the DSC data, in which at low pH only the high-temperature part of the heat capacity

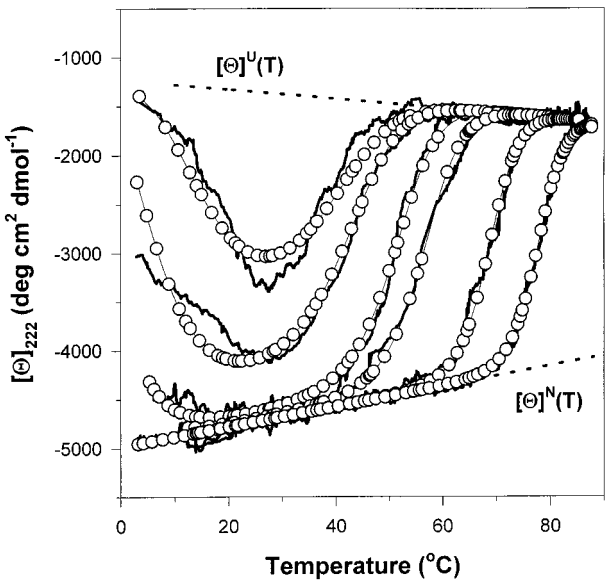

FIGURE 5: Temperature induced unfolding profiles of Trx *h* at different pHs of solution monitored by the changes in ellipticity at 222 nm. Thick lines show the actual experimental data, and dashed lines show temperature dependences of the ellipticities for the native, $[\Theta]^N(T)$, and unfolded, $[\Theta]^U(T)$, states. Open circles and thin lines show the results of the global fit of all profiles to eq 9 using parameters shown in Table 2. The experiments were performed at pH values of (from left to right) 2.0, 2.25, 2.5, 2.75, 3.0, and 3.5.

profiles is well approximated by a two-state model but not the low-temperature part. DSC measures the integral heat effect associated with the disruption of the native protein structure, both secondary and tertiary. Thus, if indeed the changes in the ellipticity in the near-UV CD represent the changes in the tertiary structure of the protein, our results indicate that the unfolding of the tertiary structure of Trx *h*, both at low and at high temperatures, is a two-state process.

Conformational Changes in Secondary Structure of Trx h Monitored by Far-UV CD Spectroscopy. The ellipticity in the far-UV CD spectrum is believed to originate from elements of the secondary structure of proteins (*51*). In particular, the ellipticity at 222 nm has been used to determine the helical content in peptides and proteins (e.g., *52, 53*). The secondary structure of Trx *h* contains more than 40% α-helices (*13, 14*). Thus, the changes in the ellipticity at 222 nm provide a useful spectroscopic probe to monitor the effects of temperature on the secondary structure of this protein.

Figure 5 shows the temperature induced changes in the ellipticity of Trx *h* at 222 nm at different pHs. At pH 2.5, 2.75, 3.0, and 3.5, the ellipticity change with temperature follows an expected sigmoidal trend. This is characteristic for the heat induced unfolding of the protein, which is accompanied by a decrease in the secondary structure content as monitored by the decrease of the absolute value of the ellipticity at 222 nm, $[\Theta]_{222}$. At four pH values obtained in the range from 2.5 to 3.5, Trx *h* has very similar values of ellipticity both at low and at high temperatures. At 20 °C, the $[\Theta]_{222}$ of Trx *h* in its native state is -4800 deg·cm^2·dmol^{-1}. The ellipticity of the native state appears to increase linearly with the increase of temperature. Similarly, the $[\Theta]_{222}$ of the unfolded state also appears to be a linear function of temperature with a small negative slope. Upon unfolding, the ellipticity of Trx *h* decreases in absolute values and reaches -1500 deg·cm^2·dmol^{-1} at 85 °C. Decreasing the pH below 2.5 does not change the observed temperature dependence of the ellipticity at high temperatures. However, at pH values of 2.0 and 2.25, the $[\Theta]_{222}$ profiles in the low temperature range clearly show the presence of cold denaturation in Trx *h*. At both pHs, the ellipticity profile has a U-shape with a minimum at ~25 °C. Increasing the temperature leads to an increase in the absolute value of $[\Theta]_{222}$, reaching the level expected for the unfolded Trx *h* at higher pH values, i.e., -1500 deg·cm^2·dmol^{-1}. Such a shape for the $[\Theta]_{222}$ dependence on temperature is an indication that Trx *h* at pH 2.0 and 2.25 undergoes cold denaturation below 25 °C and heat denaturation above 25 °C.

The temperature induced changes in the ellipticity at 222 nm obtained at different pHs were fitted simultaneously to the equation:

$$[\Theta]_{222}(T) = F_N(T)\cdot[\Theta]^N_{222}(T) + [1 - F_N(T)]\cdot[\Theta]^U_{222}(T) \quad (9)$$

where $[\Theta]^N_{222}(T)$ and $[\Theta]^U_{222}(T)$ are the ellipticities for the native and unfolded states, respectively, approximated by linear functions of temperature, and $F_N(T)$ is the temperature dependence of the population of the native protein defined by eqs 3 and 4. Thermodynamic parameters obtained from the fit of the ellipticity at 222 nm are shown in Figure 5 and in Table 2. The enthalpies of unfolding obtained from this analysis are compared to the enthalpy values obtained from DSC and near-UV CD in Figure 3. The overall correspondence of the three data sets is quite satisfactory keeping in mind that different experimental methods have been used. The major difference appears to be the transition temperature, which at the same pH was determined to be several degrees higher in the DSC experiments. This is probably related to the poorer quality of temperature measurement and control in spectroscopic experiments compared to DSC.

The quality of the fit of the experimental data to eq 2 at pH ≥2.5 is very good, indicating that under these solvent conditions the changes in $[\Theta]_{222}$ as a function of temperature can be well represented by a two-state process (Figure 5). In contrast, the fit of $[\Theta]_{222}$ profiles at pH 2.0 and 2.25 to a two-state model is clearly imperfect. The quality of the fit is particularly poor in the low-temperature range, a result similar to the one obtained from the DSC profiles. This can be interpreted as follows: at pH 2.0 and 2.25, the heat induced change in ellipticity at 222 nm of Trx *h* is a two-state process, whereas the cold induced changes in $[\Theta]_{222}$ are not. If $[\Theta]_{222}$ is directly proportional to the amount of secondary structure, there is a difference in the mechanisms of the heat and cold induced unfolding of the secondary structure of Trx *h*.

Conformational Changes in Trx h Monitored by Fluorescence Spectroscopy. To further characterize the unfolding of Trx *h*, we measured the temperature dependence of the protein Trp fluorescence. The changes in fluorescence intensity of tryptophan residues have been an important method to study conformational changes in proteins (*54*−*56*). The basis of the method is that the fluorescence emission spectrum of the indole ring of tryptophan residue strongly depends on the polarity of the milieu and thus serves as a sensitive probe for the environment of Trp residues in

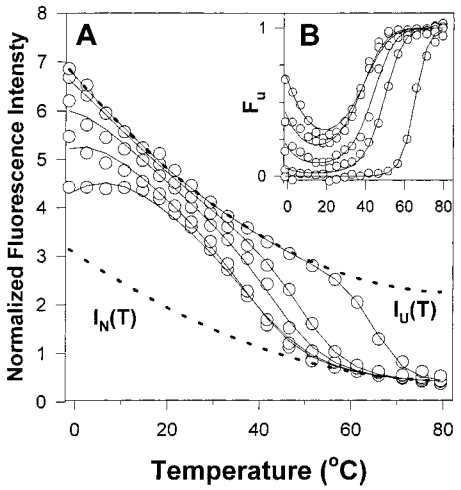

FIGURE 6: (Panel A) Temperature induced unfolding profiles of Trx *h* at different pHs monitored by the changes in Trp fluorescence intensity at 330 nm. Open circles (○) show the actual experimental data, and dashed lines show temperature dependences of the intensities for the native, $I_N(T)$, and unfolded, $I_U(T)$, states defined according to eqs 1 and 2. Thin lines show the results of the global fit of all profiles to eq 10 using the parameters shown in Table 2. The experiments were performed at pH values of (from left to right) 2.0, 2.13, 2.25, 2.5, and 3.0. (Panel B) Experimental (○) and fitted (thin lines) dependencies of the fraction of unfolded Trx *h* on temperature. The pH values are the same as in panel A.

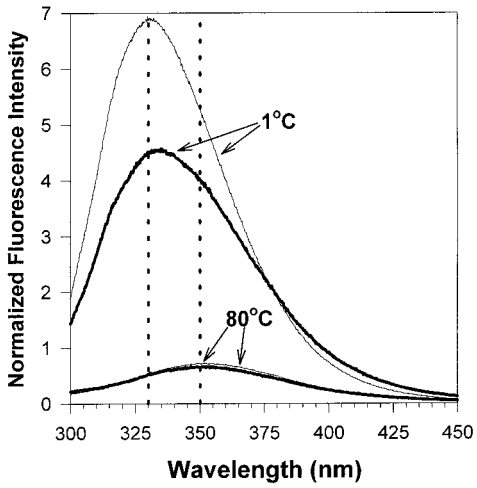

FIGURE 7: Trp fluorescence emission spectra of Trx *h* after excitation at 295 nm. The thick solid lines are for pH 2.0 and the thin solid lines for pH 3.0. The temperatures at which spectra were recorded are indicated above each profile. Dashed vertical lines show the positions of the maxima at 330 and 350 nm.

different conformational states. The Trx *h* molecule contains two tryptophan residues at positions 13 and 35: Trp13 is located in the middle of the first α-helix, and Trp35 is located in the turn connecting the second *β*-strand with the second α-helix of this typical α/*β*-protein (*13*, *14*). Thus, by monitoring the changes in the intensity of Trp fluorescence, we can obtain information about the changes in the environment of these residues upon Trx *h* unfolding. Figure 6 presents the temperature dependence of the fluorescence intensity of Trx *h* at five different pH values: 2.0, 2.13, 2.25, 2.5, and 3.0. At pHs 2.5 and 3.0, the concentration-normalized Trp fluorescence intensity follows a similar dependence both in the low-temperature range (<40 °C) where Trx *h* is still native and in the high-temperature range (>70 °C) where Trx *h* is already unfolded. The high-temperature part of the profiles is not influenced by decreasing the pH to 2.25 or even 2.0. The low-temperature parts of the Trp fluorescence intensity profiles obtained at pH ≤2.25 are very different, indicating that Trp residues in Trx *h* at low pH change their fluorescence intensity in a different way than at pH ≥2.5, possibly because of cold denaturation of the protein.

The fit of the Trp-fluorescence intensity profiles was performed according to a two-state model as

$$I(T) = F_N(T)\cdot I_N(T) + [1 - F_N(T)]\cdot I_U(T) \qquad (10)$$

where $I_N(T)$ and $I_U(T)$ are the temperature dependencies of the Trp fluorescence intensities in the native and unfolded states, respectively, and $F_N(T)$ is the temperature dependence of the population of the native protein defined by eqs 3 and 4. Analyzing the data presented in Figure 6 is not simple per se due to the strong temperature dependence of the tryptophan fluorescence. To avoid ambiguity in the estimates of the temperature dependences for the fluorescence of the native and unfolded states, we used the model compound *N*-acetyl-L-tryptophanamide (NATA) as described (see Materials and Methods). The thermodynamic parameters calculated from the fit of the data are presented in the Table 2. The enthalpies of unfolding obtained from the Trp fluorescence melting profiles compare well with the enthalpies obtained using other spectroscopic methods and DSC (Figure 3). Nevertheless, as already observed in the case of the two-state fit of the DSC and far-UV CD profiles, the quality of the fit is reasonably good at pH above 2.5 and not very good at pH 2.0, 2.13, and 2.25. Although the error of the analysis of temperature dependence of the fluorescence intensity profiles is significantly larger than for the other methods (DSC and far- and near-UV CD spectroscopies), it is clear that the changes in the environment of tryptophan residues in the molecule of Trx *h* follow closely a two-state process only upon heat denaturation.

Additional support for this conclusion stems from the analysis of the temperature dependence of the maximum of the fluorescence emission spectrum of Trx *h*. The fluorescence emission maximum of tryptophan in a polar environment such as water is at 350 nm (*55*, *56*). In a less polar environment, there is a significant blue shift of up to 20 nm (λ_{max} = 330 nm). Figure 7 compares the fluorescence emission spectra of Trx *h* at pH 2.0 and 3.0 at low (1 °C) and high (80 °C) temperatures. At pH 3.0 where no cold denaturation is observed, the fluorescence emission spectrum at 1 °C has a maximum at 330 nm which suggests that Trp residues are in a nonpolar environment, presumably buried in the native state. When the temperature increases, the Trx *h* molecule unfolds, leading to a red shift in the maximum of the emission spectrum from 330 to 350 nm at 80 °C and pH 3.0. This 20 nm red-shift in the emission maximum of Trp fluorescence is probably the result of a more extensive exposure of Trp residues to the solvent in the unfolded state. Similarly, the emission spectrum of Trx *h* at pH 2.0 and 80 °C has a maximum at 350 nm, again indicating that under these conditions Trp residues are solvent-exposed. It is important to note that at 80 °C the emission maxima are similar at pH 2.0 and 3.0. The concentration-normalized Trp fluorescence intensities are also very similar, which indicates that the state populated at high temperature is the same for

these two pHs. At low-temperature, however, the Trp fluorescence emission spectra of Trx *h* in pH 2.0 and pH 3.0 differ significantly. At pH 2.0 and 1 °C, Trx *h* is expected to be largely unfolded, as was already shown by the near- and far-UV CD and fluorescence intensity data. So, it will be expected that under these conditions (1 °C, pH 2.0) the intensity of Trp fluorescence will be lower and the emission spectrum of Trx *h* will have a maximum corresponding to the solvent-exposed Trp, i.e., close to 350 nm. In contrast, the maximum of Trp fluorescence is at 335 nm, a value only slightly higher than the 330 nm maximum observed for the native state of Trx *h*.

This difference in the maximum in the fluorescence emission spectrum of Trx *h* supports our earlier observations using other (DSC, near- and far-UV CD, and steady-state Trp fluorescence) techniques; i.e., the mechanism of cold denaturation of Trx *h* is different from the mechanism of heat denaturation. This raises the following question: Why are the molecular mechanisms governing these two processes different?

Mechanism of Cold Denaturation of Trx h. Four (DSC, far-UV CD, fluorescence intensity, and Trp emission maximum) out of five biophysical methods show that the cold induced denaturation of Trx *h* is not a two-state process. Only the melting profiles obtained using near-UV CD spectroscopy show that both cold and heat denaturation profiles could be two-state. The near-UV CD spectroscopy follows only the overall global changes in the tertiary interactions. The far-UV CD spectroscopy, on the other hand, indicates that the changes in the secondary structure upon cold denaturation are not two-state. Similarly, the results of DSC and fluorescence spectroscopy indicate that cold denaturation of Trx *h* is more complex than two-state. The intermediate state populated upon cold denaturation of Trx *h* does not seem to be similar to that of the so-called "molten globule" state (*57*). In the molten globule state, the tertiary structure is lost but a large fraction of secondary structure remains intact. This clearly is not the case for Trx *h*. For example, at pH 2.0 and 0 °C according to the far-UV CD, 100% of the Trx *h* molecules are unfolded (Figure 5). However, according to near-UV CD (Figures 4A,B), fluorescence (Figure 6), or DSC (Figure 2), Trx *h* is only 70−80% unfolded. Thus, it is likely that the intermediate state is not a molten globule state. It rather resembles a collapsed state which is characterized by the absence of specific secondary and tertiary structures, but with aromatic residues remaining largely buried [see, e.g., (*58*−*60*)]. This is supported by the fact that the fluorescence emission maximum of the cold-denatured state of Trx h at pH 2.0 is at 335 nm, typical for tryptophans that are buried in a nonaqueous environment.

It is possible that the native state of Trx *h* consists of at least two different states. Such a situation has been described for the *E. coli* thioredoxin (*61*). Using urea gradient gel electrophoresis, Langsetmo et al. have shown that this protein folds into two compact forms that have different stability. The differences in stability of the two compact forms of *E. coli* Trx are more pronounced at low temperature (2 °C) than at 25 °C. These two compact forms of *E. coli* thioredoxin differ in the conformation of the highly conserved proline residue (Pro76 in *E. coli* Trx and Pro80 in Trx *h*) which can exist in the cis or trans forms in the native state. This highly conserved Pro residue is present in the sequence of Trx *h*

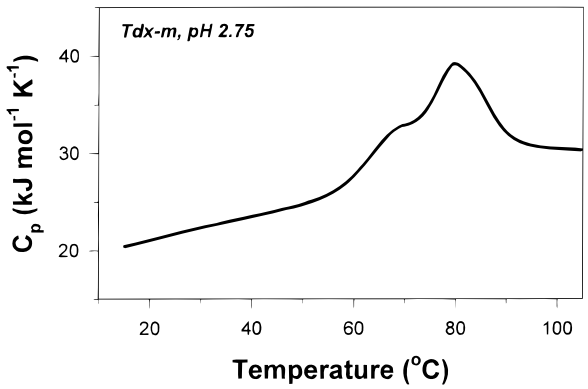

FIGURE 8: Temperature dependence of the partial molar heat capacity of thioredoxin, *m*, in solution at pH 2.75.

(Pro80) and is also in the cis conformation in the native state (*14*). It is conceivable that Trx *h* also exists in two compact forms that are cis−trans isoforms of Pro80 which could have different stabilities.

Alternatively, the mechanism of cold denaturation of Trx *h* may be similar to that of phosphoglycerate kinase (*49*). Griko et al. have shown that phosphoglycerate kinase consists of two domains which strongly cooperate at high temperature and thus unfold simultaneously in a single two-state transition. At low temperatures, the balance of forces that cooperate these two domains changes, and they unfold as two independent two-state transitions (*62*). In the case of phosphoglycerate kinase, the intrinsic stabilities of the individual domains are very different, and unfolding of individual domains can be observed independently. Griko et al. have shown that cold denaturation is a three-state unfolding, with the N-terminal domain being less stable and unfolding before the C-terminal domain. Thus, we propose that the Trx *h* molecule also consists of two domains, but in contrast to phosphoglycerate kinase the stabilities of these domains are not significantly different and thus their cold denaturation transitions are not well separated due to the overlap.

It will require use of site-directed mutagenesis to affect the stability of one of the domains relative to the other to be able to observe directly their independent unfolding. That such an approach is feasible can be anticipated from the DSC study of the heat denaturation of thioredoxin *m* (Trx *m*) from *Chlamydomonas reinhardtii*. Sequence homology between Trx *h* and Trx *m* is about 50%, and structural similarity is even higher (*1*); however, the unfolding of Trx *m* clearly shows a three-state process (Figure 8).

ACKNOWLEDGMENT

We thank Dr. Marimar Lopez for help with the fluorescence experiments and valuable comments on the manuscript.

REFERENCES

1. Jacquot, J. P., Lancelin, J. M., and Meyer, Y. (1997) *New Phytol. 136*, 543−570.
2. Mark, D. F., and Richardson, C. C. (1976) *Proc. Natl. Acad. Sci. U.S.A. 73*, 780−784.
3. Holmgren, A. (1995) *Structure 3*, 239−243.
4. Martin, J. L. (1995) *Structure 3*, 245−250.
5. Dyson, H. J., Holmgren, A., and Wright, P. E. (1988) *FEBS Lett. 228*, 254−258.

6. Dyson, H. J., Gippert, G. P., Case, D. A., Holmgren, A., and Wright, P. E. (1990) *Biochemistry 29*, 4129−4136.
7. Katti, S. K., LeMaster, D. M., and Eklund, H. (1990) *J. Mol. Biol. 212*, 167−184.
8. Jeng, M. F., Campbell, A. P., Begley, T., Holmgren, A., Case, D. A., Wright, P. E., and Dyson, H. J. (1994) *Structure 2*, 853−868.
9. Forman-Kay, J. D., Clore, G. M., Driscoll, P. C., Wingfield, P., Richards, F. M., and Gronenborn, A. M. (1989) *Biochemistry 28*, 7088−7097.
10. Forman-Kay, J. D., Clore, G. M., Wingfield, P. T., and Gronenborn, A. M. (1991) *Biochemistry 30*, 2685−2698.
11. Qin, J., Clore, G. M., Kennedy, W. P., Kuszewski, J., and Gronenborn, A. M. (1996) *Structure 4*, 613−620.
12. Stein, M., Jacquot, J. P., Jeannette, E., Decottignies, P., Hodges, M., Lancelin, J. M., Mittard, V., Schmitter, J. M., and Miginiac-Maslow, M. (1995) *Plant Mol. Biol. 28*, 487−503.
13. Mittard, V., Morelle, N., Brutscher, B., Simorre, J. P., Marion, D., Stein, M., Jacquot, J. P., Lirsac, P. N., and Lancelin, J. M. (1995) *Eur. J. Biochem. 229*, 473−485.
14. Mittard, V., Blackledge, M. J., Stein, M., Jacquot, J. P., Marion, D., and Lancelin, J. M. (1997) *Eur. J. Biochem. 243*, 374−383.
15. Nicastro, G., De Chiara, C., Pedone, E., Tato, M., Rossi, M., and Bartolucci, S. (2000) *Eur. J. Biochem. 267*, 403−413.
16. Alam, J., Curtis, S., Gleason, F. K., Gerami-Nejad, M., and Fuchs, J. A. (1989) *J. Bacteriol. 171*, 162−171.
17. Reutimann, H., Straub, B., Luisi, P. L., and Holmgren, A. (1981) *J. Biol. Chem. 256*, 6796−6803.
18. Wilson, J., Kelley, R. F., Shalongo, W., Lowery, D., and Stellwagen, E. (1986) *Biochemistry 25*, 7560−7566.
19. Hiraoki, T., Brown, S. B., Stevenson, K. J., and Vogel, H. J. (1988) *Biochemistry 27*, 5000−5008.
20. Lin, T. Y., and Kim, P. S. (1989) *Biochemistry 28*, 5282−5287.
21. Langsetmo, K., Fuchs, J. A., Woodward, C., and Sharp, K. A. (1991) *Biochemistry 30*, 7609−7614.
22. Ladbury, J. E., Wynn, R., Hellinga, H. W., and Sturtevant, J. M. (1993) *Biochemistry 32*, 7526−7530.
23. Ladbury, J. E., Kishore, N., Hellinga, H. W., Wynn, R., and Sturtevant, J. M. (1994) *Biochemistry 33*, 3688−3692.
24. Georgescu, R. E., Li, J. H., Goldberg, M. E., Tasayco, M. L., and Chaffotte, A. F. (1998) *Biochemistry 37*, 10286−10297.
25. Georgescu, R. E., Braswell, E. H., Zhu, D., and Tasayco, M. L. (1999) *Biochemistry 38*, 13355−13366.
26. Hellinga, H. W., Wynn, R., and Richards, F. M. (1992) *Biochemistry 31*, 11203−11209.
27. Wynn, R., and Richards, F. M. (1993) *Protein Sci. 2*, 395−403.
28. Desjarlais, J. R., and Handel, T. M. (1995) *Protein Sci. 4*, 2006−2018.
29. Lemaire, S. D., Richardson, J. M., Goyer, A., Keryer, E., Lancelin, J. M., Makhatadze, G. I., and Jacquot, J. P. (2000) *Biochim. Biophys. Acta 1476*, 311−323.
30. Gill, S. C., and von Hippel, P. H. (1989) *Anal. Biochem. 182*, 319−326.
31. Pace, C. N., Vajdos, F., Fee, L., Grimsley, G., and Gray, T. (1995) *Protein Sci. 4*, 2411−2423.
32. Winder, A. F., and Gent, W. L. (1971) *Biopolymers 10*, 1243−1251.
33. Gribenko, A. V., and Makhatadze, G. I. (1998) *J. Mol. Biol. 283*, 679−694.
34. Richardson, J. M., McMahon, K. W., MacDonald, C. C., and Makhatadze, G. I. (1999) *Biochemistry 38*, 12869−12875.
35. Lopez, M. M., Yutani, K., and Makhatadze, G. I. (1999) *J. Biol. Chem. 274*, 33601−33608.
36. Plotnikov, V. V., Brandts, J. M., Lin, L. N., and Brandts, J. F. (1997) *Anal. Biochem. 250*, 237−244.
37. Makhatadze, G. I., Medvedkin, V. N., and Privalov, P. L. (1990) *Biopolymers 30*, 1001−1010.
38. Makhatadze, G. I. (1998) *Biophys. Chem. 71*, 133−156.
39. Pace, C. N., Grimsley, G. R., Thomas, S. T., and Makhatadze, G. I. (1999) *Protein Sci. 8*, 1500−1504.
40. Makhatadze, G. I. (1998) *Measuring protein thermostability by differential scanning calorimetry*, Vol. 2, John Wiley & Sons, New York.
41. Ibarra-Molero, B., Makhatadze, G. I., and Sanchez-Ruiz, J. M. (1999) *Biochim. Biophys. Acta 1429*, 384−390.
42. Sanchez-Ruiz, J. M. (1992) *Biophys. J. 61*, 921−935.
43. Santoro, M. M., and Bolen, D. W. (1992) *Biochemistry 31*, 4901−4907.
44. Bartolucci, S., Guagliardi, A., Pedone, E., De Pascale, D., Cannio, R., Camardella, L., Rossi, M., Nicastro, G., de Chiara, C., Facci, P., Mascetti, G., and Nicolini, C. (1997) *Biochem. J. 328*, 277−285.
45. Privalov, P. L., Griko Yu, V., Venyaminov, S., and Kutyshenko, V. P. (1986) *J. Mol. Biol. 190*, 487−498.
46. Griko, Y. V., Privalov, P. L., Sturtevant, J. M., and Venyaminov, S. (1988) *Proc. Natl. Acad. Sci. U.S.A. 85*, 3343−3347.
47. Griko, Y. V., Privalov, P. L., Venyaminov, S. Y., and Kutyshenko, V. P. (1988) *J. Mol. Biol. 202*, 127−138.
48. Griko, Y. V., and Privalov, P. L. (1992) *Biochemistry 31*, 8810−8815.
49. Griko Yu, V., Venyaminov, S., and Privalov, P. L. (1989) *FEBS Lett. 244*, 276−278.
50. Privalov, P. L. (1990) *Crit. Rev. Biochem. Mol. Biol. 25*, 281−305.
51. Woody, R. W. (1995) *Methods Enzymol. 246*, 34−71.
52. Pain, R. (1996) in *Current Protocols in Protein Science*, pp 761−723, John Wiley & Sons, New York.
53. Scholtz, J. M., and Baldwin, R. L. (1992) *Annu. Rev. Biophys. Biomol. Struct. 21*, 95−118.
54. Lakowitcz, J. R. (1983) *Principles of Fluorescence Spectroscopy*, Plenum Press., New York.
55. Eftink, M. R. (1994) *Biophys. J. 66*, 482−501.
56. Eftink, M. R., and Shastry, M. C. (1997) *Methods Enzymol. 278*, 258−286.
57. Ptitsyn, O. B. (1995) *Adv. Protein Chem. 47*, 83−229.
58. Fink, A. L. (1995) *Annu. Rev. Biophys. Biomol. Struct. 24*, 495−522.
59. Privalov, P. L. (1996) *J. Mol. Biol. 258*, 707−725.
60. Houry, W. A., and Scheraga, H. A. (1996) *Biochemistry 35*, 11734−11746.
61. Langsetmo, K., Fuchs, J., and Woodward, C. (1989) *Biochemistry 28*, 3211−3220.
62. Freire, E., Murphy, K. P., Sanchez-Ruiz, J. M., Galisteo, M. L., and Privalov, P. L. (1992) *Biochemistry 31*, 250−256.

BI000610B